POLISH MARITIME RESEARCH 4 (128) 2025 Vol. 32; pp. 132-141
10.2478/pomr-2025-0056

Experimental and Numerical Investigation of the Stiffness of the FPR Composite Mast of an A-Class Catamaran (A-Cat) with Sensitivity Analysis

Tomasz Ferenc [1,*]
Tomasz Mikulski [2]
[1] Gdansk University of Technology, Faculty of Civil and Environmental Engineering, Gdansk, Poland
[2] Gdansk University of Technology, Faculty of Ocean Engineering and Ship Technology, Gdansk, Poland

* Corresponding author: *tomasz.ferenc@pg.edu.pl (Tomasz Ferenc)*

ABSTRACT

The paper presents an experimental and numerical investigation of the stiffness of an A-class catamaran (A-Cat) mast. The structure has a constant, prismatic cross-section and is made from fibre-reinforced plastic (FRP) multilayered laminate. The material parameters of the structure were identified. Then, static tests were conducted using a simply supported beam configuration, where supports were established at the beginning of the mast length and at the rigging attachment point. A computational model of the mast was created and analysed using the finite element method (FEM). A sensitivity analysis was performed on a validated model, from which sensitivity coefficients were obtained. On this basis, it was possible to determine how the structure could be modified to obtain the expected deformation, i.e. the maximum displacement of a selected point on the mast or the shape of the mast bending under a given load.

Keywords: A-class catamaran, mast, experimental and numerical investigation, sensitivity analysis, FRP laminates

INTRODUCTION

The mast is the most important element of the rigging. It should have the right profile and cross-sectional shape to obtain adequate strength and stiffness. On the one hand, it has to prevent breakage and high deflection in strong winds, but on the other hand, excessive stiffness has to be avoided in order to fulfil mass requirements. The mast structure determines the ability to shape the sail and its efficiency. Finding the right mast-sail combination is a key factor in ensuring efficient sailing [1-4].

Selecting the right mast, especially in competitive sailing, is a complex process. Depending on the boat class, the rigging is constructed differently. For example, in the Finn class, the mast operates in a cantilever configuration with the ability to rotate around a vertical axis. In the case of Olympic-class catamarans such as the Nacra 17 [5,6], 470-class boats [7,8], or A-class catamarans (A-Cats) [9,10], the mast is connected to standing rigging, which provides additional support for the mast. The method and sequence of tensioning the rigging may also be the subject of research [11]. Masts can also be manufactured from various materials, primarily aluminium and fibre-reinforced plastic (FRP). In the case of FRP, the mast structure is a multilayer laminate composed of unidirectional or multidirectional carbon fabrics, saturated with polymer resins such as epoxy. Additionally, there are masts with a constant, prismatic cross-section along the length and masts with a variable cross-section along the length, known as tapered masts.

In mast design, a key factor is the distribution of stiffness along the mast's length, in both the fore/aft (F/A) and sideways (S) directions. This can be influenced by factors such as the standing rigging, the shape of the mast's cross-section, the material the mast is made from, or the manufacturing process itself [12-15]. With a mast made from FRP, variable stiffness can be achieved by varying the stack sequence of the laminate, inserting additional reinforcing layers in appropriately selected zones along the mast's length. This option is commonly used in the production of competition boat masts. For example, in the Finn class, a competitor provides the manufacturer with the mast's bending characteristics in two perpendicular directions; this is considered the standard bending test scheme. Not only is the mast's top deflection important, but also the shape of the bending deflection line, measured at three additional points along the mast's length (Fig. 1), is crucial. The measurement points are established at 1/4, 1/2, and 3/4 of the mast length, counting from the measurement band (mast mounting), where the distance between the deformed mast and the cut connecting the mast support and its end is determined. An example of deflection values under such a test is given in Table 1.

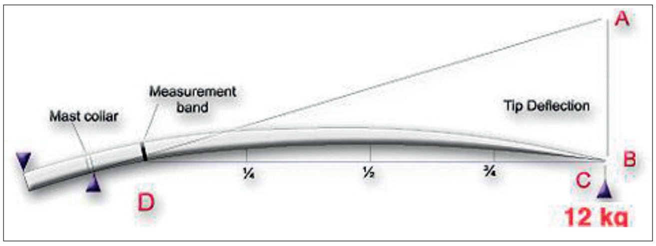

Fig. 1. Scheme of measurement in standard bending test (http://www.finn-masters.pl/bud_maszt.htm)

Tab. 1. Mast deflection under static test

	1/4	1/2	3/4	Tip
Deflection in F/A direction [mm]	87	117	91	500
Deflection in S direction [mm]	75	117	107	375

The main aims of conducting a static evaluation of the mast depending on the rigging type are the following:

– the verification of the mast stiffness characteristics provided by the manufacturer,
– the identification of the stiffness distribution along the mast length,
– the diagnosis of any loss of mast stiffness after a specified period of use.

Today, more demanding fluid–structure interaction (FSI) analyses are becoming increasingly popular [16-20]. These analyses examine the interaction between the structure and the flow of the medium (water or air) around it. This makes it possible to simulate the structure's operation under conditions close to reality. However, these calculations are very time- and hardware-intensive. Furthermore, structural data are required parameters of the structure for the best representation.

Another important factor that has to be considered during the mast design process is the effect of time on its parameters, such as strength. Cyclic loading that occurs during sailing reduces the material strength, which can lead to damage or even the failure of the entire mast [21]. Moreover, in the case of high-performance boats, fatigue effects can also cause a reduction in the mast's stiffness.

The paper addresses the diagnostics of the FRP mast of an A-class catamaran (A-Cat). Static tests were conducted using a simply supported beam configuration, where supports were established at the beginning of the mast length and at the rigging attachment point. The material parameters of the mast, which had a constant, prismatic cross-section along the mast's length, were identified. A computational model of the mast was created and analysed using the finite element method (FEM). Based on this model, the sensitivity analysis apparatus was used [22-24]; this involves estimating sensitivity coefficients that quantify the influence of a group of inputs (so-called design variables) on the output (so-called state variable). This allowed us to determine how to modify the mast to obtain the required deformation under the specified load. The results obtained from the analysis may be used in more sophisticated FSI analysis as well.

DESCRIPTION OF THE MAST

The analysed mast is a thin-wall composite structure with a closed round cross-section. The precise shape and dimensions are presented in Fig. 2, while the overall view is presented in Fig. 3. The width and height of the cross-section are 60 mm and 145 mm, respectively. The length of the mast is 9 m, and it is supported at two points – at one end and after 6.3 m. At the first point, the mast is connected to the catamaran, and at the other point, the rigging is attached to the structure.

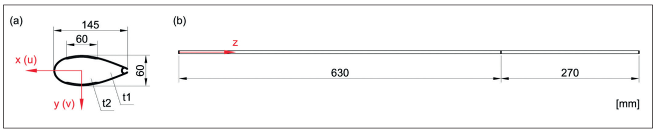

Fig. 2. Dimensions of the mast: (a) cross-section, (b) side view

The mast is made of a multilayered FRP laminate with carbon and glass fibre reinforcement and polymer resin [25,26]. Three types of fabrics were used: glass two-directional fabric F204 with a density of 204 g/m^2, carbon unidirectional fabric UD300 (300 g/m^2), and carbon two-directional fabric BX400 (200 + 200 g/m^2). Two types of stack sequences were used. The first and main type (type *t*1) consists of five fabric layers

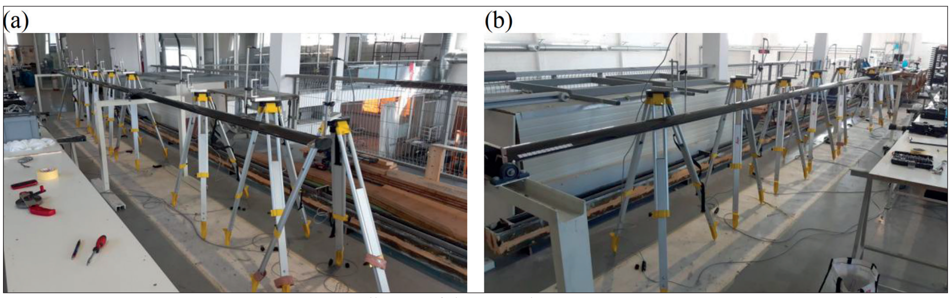

Fig. 3. Overall view of the mast during experiments

and, from the outer side, is as follows: [F204/BX400/$(UD300)_2$/BX400]. The total thickness of the laminate (*t*1) is 2.0 mm. The second type (type *t*2) is related to the increase of the cross-sectional stiffness in the horizontal direction, along the y-axis. Thus, on the cross-section sides, extra layers of unidirectional fabrics are inserted, and the stack sequence is as follows: [F204/BX400/(UD300)4/BX400]. The total thickness of the laminate (*t*2) is 3.5 mm.

The material properties of whole laminates were investigated in a unidirectional tensile test on a Zwick Roell testing machine. Test samples with dimensions 25 × 250 mm were cut from panels manufactured by the producer using the same technology used to manufacture the mast. The general principles for conducting experiments were taken from the ISO 527-1 and ISO 527-4 standards. The initial force was assumed to be at the level of 200 N. The experiments were performed at a constant traverse speed of 2 mm/minute. The extensometer was used to measure strains in longitudinal and transverse directions in the middle of the investigated specimen length. Five specimens of types *t*1 and *t*2 were examined, respectively. The mean values of the stiffness modulus and Poisson's ratio obtained in the longitudinal direction (along the z-axis) are listed in Table 2.

Tab. 2. Material properties of laminate types t1 and t2

	Laminate type *t*1	Laminate type *t*2
Stiffness modulus [GPa]	48.9	93.5
Poisson's ratio [-]	0.167	0.166
Maximum stress (strength) [MPa]	595	727

According to the design standards, both the ultimate limit state (ULS) and serviceability limit state (SLS) have to be considered in order to evaluate the structure. However, in composite structures, the extreme stress value is usually relatively small compared to its strength. The stress level can be assessed by controlling the index failure (IF) according to different hypotheses, i.e. the Tsai-Wu hypothesis [27,28], in which the IF cannot exceed a value of 0.2. Thus, the SLS becomes more significant to verify.

The key parameter during the exploitation of the masts is their flexural stiffness along their length in both directions: horizontally, which is also known as the sides (S) direction, along the *y*-axis (*v*-axis), and vertically, in the so-called fore/aft (F/A) direction along the *x*-axis (*u*-axis), shown in Fig. 2. Furthermore, due to different wind speeds at different heights above the water surface, masts are often designed to have varying stiffness along their lengths. Hence, the appropriate design and manufacturing of the mast become extremely significant.

EXAMINATION OF THE MAST

EXPERIMENT SET-UP

During the experiments, the mast was supported at two points, at one end and after 6.3 m from this end; this is related to the support conditions of a mast installed in a catamaran. To conduct experiments, steel supports were designed and manufactured with specially matched elements that allow mast rotations. Moreover, these elements allow us to choose the mast orientation, whether its cross-section is positioned along the S direction or along the F/A direction. Thus, the behaviour in two directions can be investigated, as presented in Fig. 4.

For both mast orientations, three static load cases were applied to investigate the mast behaviour: *lc*1, *lc*2, and *lc*3. In scheme *lc*1 (Fig. 5), the force was applied at the end of the mast, while in scheme *lc*2, it was applied at the mid-length between supports. Additionally, in scheme *lc*3, two forces were applied that correspond to both scheme *lc*1 and scheme *lc*2; hence, *lc*3 = *lc*2 + *lc*1.

During the experiments, eight HBM WA100 inductive sensors, with the HBM Data Acquisition System MX 840A, were installed and used to measure displacement. The measuring points were placed at about 1 m intervals and are shown in Fig. 5. As the mast was investigated in two cross-section positions, the measured values of displacement are described as *v*1−*v*8 and *u*1−*u*8 for the S and F/A directions, respectively.

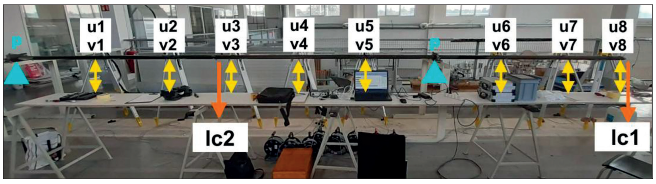

Fig. 5. Conducted load schemes: lc1 and lc2

RESULTS FOR MAST CROSS-SECTION ALONG S DIRECTION

First, the mast was investigated with a cross-section in position S (along the *y*-axis) (Fig. 4a). For schemes *lc*1 and *lc*2, a force with a value of 196.2 N (20 kg) was applied in four steps: 25%, 50%, 75%, and 100% of the final value. For scheme *lc*3, the two forces were applied in one step, with values of 50% of the force applied in scheme *lc*1 and 100% of the force applied in scheme *lc*2. Thus, the two forces were applied with the following values: 98.10 N

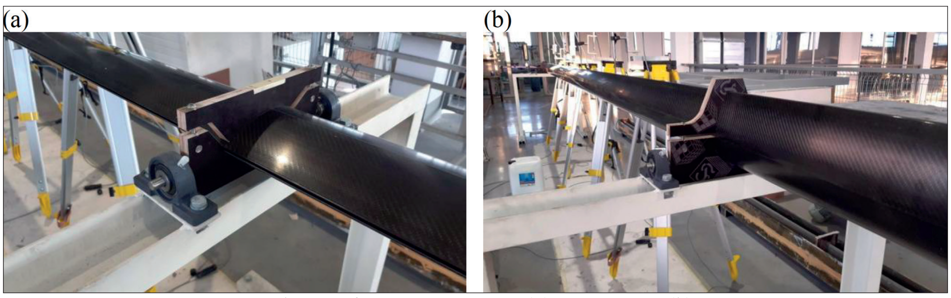

Fig. 4. Supporting elements for mast positioning: (a) in position S, (b) in position F/A

Tab. 3. Measured values at points v1–v8 under load schemes lc1–lc3 for the cross-section along the S direction

F / m	*p*	*v*1	*v*2	*v*3	*v*4	*v*5	*p*	*v*6	*v*7	*v*8
[N] / [kg]	-	[mm]	[mm]	[mm]	[mm]	[mm]	-	[mm]	[mm]	[mm]
*lc*1										
49.05 / 5	-	3.31	5.68	6.94	6.72	4.51	-	-7.97	-18.44	-27.33
98.10 / 10	-	6.95	11.70	14.36	13.87	9.30	-	-16.16	-37.90	-55.62
147.15 / 15	-	11.06	18.50	22.63	21.76	14.55	-	-25.07	-58.63	-85.94
196.20 / 20	-	14.78	24.75	30.12	28.90	19.36	-	-33.42	-77.82	-114.13
*lc*2										
49.05 / 5	-	-2.95	-4.64	-5.17	-4.09	-2.16	-	1.81	3.50	4.46
98.10 / 10	-	-6.49	-10.17	-11.44	-9.18	-4.92	-	4.46	8.91	11.71
147.15 / 15	-	-10.36	-16.34	-18.28	-14.80	-8.02	-	7.58	15.34	20.62
196.20 / 20	-	-13.83	-21.92	-24.39	-19.69	-10.69	-	10.08	20.29	27.21
*lc*3										
98.10+196.20 / 10+20	-	-6.92	-10.44	-10.33	-6.28	-1.73	-	-5.16	-15.90	-25.78

(10 kg) and 196.2 N (20 kg), respectively. The measured values of displacement at points *v*1–*v*8 under load schemes *lc*1–*lc*3 are listed in Table 3.

The deformation of the mast under each conducted load scheme – *lc*1, *lc*2, and *lc*3 – is presented in Fig. 6–Fig. 8, respectively. In addition to the values obtained at points *v*1–*v*8, the interpolation is shown as well. Furthermore, Fig. 8 presents a comparison of the values obtained during load scheme *lc*3 and the sum of the values measured during schemes *lc*1 and *lc*2.

The maximum displacement caused by the force is equal to 196.2 N (20 kg), taking a value of about 114.1 mm at the mast top for scheme *lc*1. On the other hand, for scheme *lc*2, the extreme displacements are about 24.4 mm and 27.2 mm at the mid-length of the mast and at its top, respectively.

RESULTS FOR MAST CROSS-SECTION ALONG F/A DIRECTION

Second, the mast was examined with a cross-section orientated in the F/A direction (along the *x*-axis) (Fig. 4b). Three schemes – *lc*1, *lc*2, and *lc*3 – were conducted, with forces applied analogously to the previously described experiments. The measured values of displacement at points *u*1–*u*8 under load schemes *lc*1–*lc*3 are listed in Table 4. Additionally, the deformation of the mast under conducted load schemes *lc*1, *lc*2, and *lc*3 is presented in Fig. 9–Fig. 11.

The displacement exceeded values of about 51.4 mm at the mast top for scheme *lc*1, about 10.9 mm in the middle of the mast length, and about 11.4 mm at the mast top for scheme *lc*2.

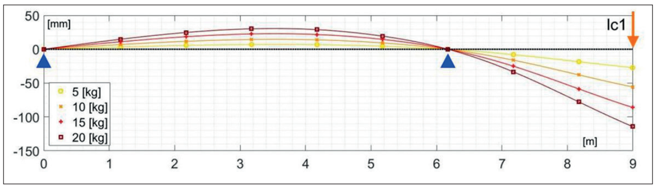

Fig. 6. The mast deformation under load scheme lc1 with cross-section along the S direction

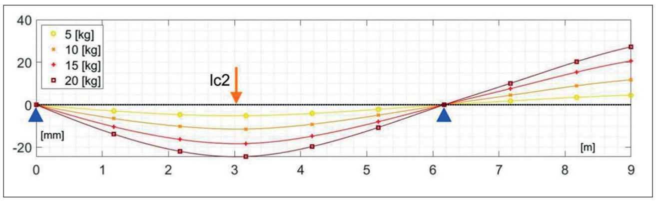

Fig. 7. The mast deformation under load scheme lc2 with cross-section along the S direction

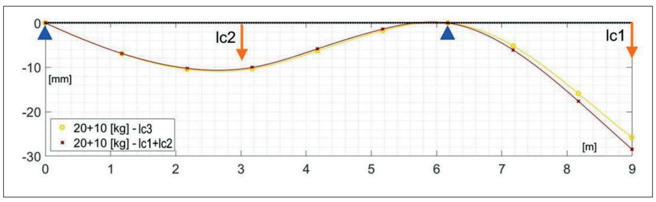

Fig. 8. The mast deformation under load scheme lc3 with cross-section along the S direction

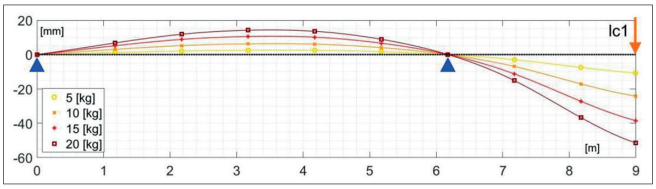

Fig. 9. The mast deformation under load scheme lc1 with cross-section along the F/A direction

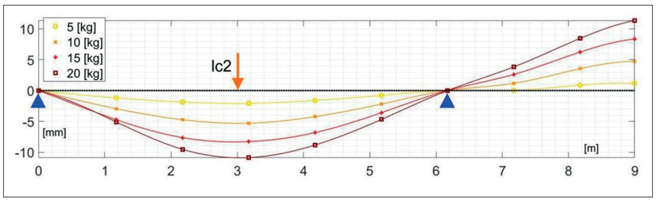

Fig. 10. The mast deformation under load scheme lc2 with cross-section along the F/A direction

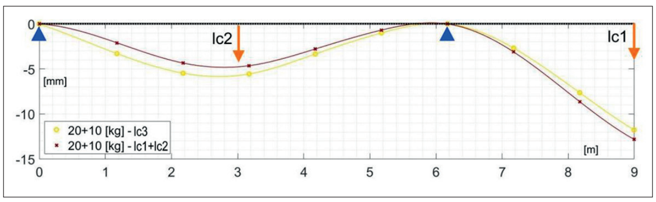

Fig. 11. The mast deformation under load scheme lc3 with cross-section along the F/A direction

Tab. 4. Measured values at points u1–u8 under load schemes lc1–lc3 for the cross-section along the F/A direction

F / m	*p*	*u*1	*u*2	*u*3	*u*4	*u*5	*p*	*u*6	*u*7	*u*8
[N] / [kg]	-	[mm]	[mm]	[mm]	[mm]	[mm]	-	[mm]	[mm]	[mm]
					*lc*1					
49.05 / 5	-	1.15	2.05	2.51	2.47	1.69	-	-3.00	-7.50	-10.76
98.10 / 10	-	3.01	5.22	6.25	6.07	4.02	-	-6.95	-17.09	-24.19
147.15 / 15	-	5.16	8.82	10.51	10.12	6.62	-	-11.29	-27.23	-38.47
196.20 / 20	-	6.77	11.82	14.16	13.54	8.89	-	-15.17	-36.71	-51.38
					*lc*2					
49.05 / 5	-	-1.20	-1.87	-2.08	-1.61	-0.80	-	0.03	0.87	1.16
98.10 / 10	-	-2.95	-4.74	-5.31	-4.23	-2.20	-	1.19	3.55	4.74
147.15 / 15	-	-4.74	-7.65	-8.29	-6.82	-3.60	-	2.62	6.24	8.36
196.20 / 20	-	-5.11	-9.56	-10.88	-8.85	-4.70	-	3.84	8.46	11.38
					*lc*3					
98.10+196.20 / 10+20	-	-3.29	-5.46	-5.55	-3.33	-1.00	-	-2.68	-7.64	-11.76

COMPUTATIONAL MODEL OF THE MAST

DESCRIPTION OF THE MODEL

The computational model of the mast was built in FEMAP with Nastran software using the FEM. In order to simulate mast behaviour under static loading schemes *lc*1 and *lc*2, the laminates were modelled by means of four-node shell elements with linear shape functions and full integration. Although the mast consists of a multilayer laminate, the equivalent single layer (ESL) theory was applied, which allows the laminate to be represented by a single-layered shell of equivalent properties. This approach allows us to simulate the global behaviour of the structure with simple and fast calculations. On the other hand, the method has its limitations and ignores phenomena resulting from the multilayer nature of the laminate, such as ply-by-ply stress distributions, delamination, and interlaminar shear, and it is not suiTable for local damage and fracture analyses. Moreover, due to the geometry of the mast, in which the length dimension is much greater than the dimensions of the cross-section, the material properties in the longitudinal direction are crucial. Thus, the isotropic material was adopted to model the structure with the values of properties given in Table 2.

The geometry of the model is identical to that of the real structure given in Fig. 2. Due to the cross-section dimensions, the characteristic size of the finite element was assumed to be 0.005 m (Fig. 12). Hence, the total number of elements and the total number of nodes were equal to 133773 and 133962, respectively. The boundary conditions were considered to be as described in the previous section. However, only the maximum values of loads equal to 196.2 N (20 kg) were assumed in both load schemes.

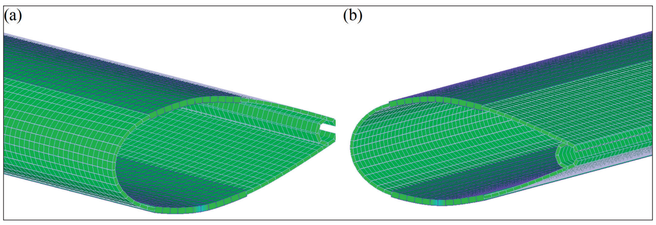

Fig. 12. Overall view of the model with shell elements and visualised thickness

RESULTS AND COMPARISON WITH EXPERIMENTS

In order to validate the numerical model of the mast, its deformation was compared with the experiment. Both mast orientations were examined under two load schemes, *lc*1 and *lc*2. The deformation of the mast in the S and F/A directions is presented in Fig. 13a–d for schemes *lc*1 and *lc*2, respectively. The red line represents the model, while the squares represent the measuring points *u*1–*u*8 or *v*1–*v*8. Additionally, the values at the measuring points were compared (including the determination of the relative error) and are listed in Table 5 and Table 6.

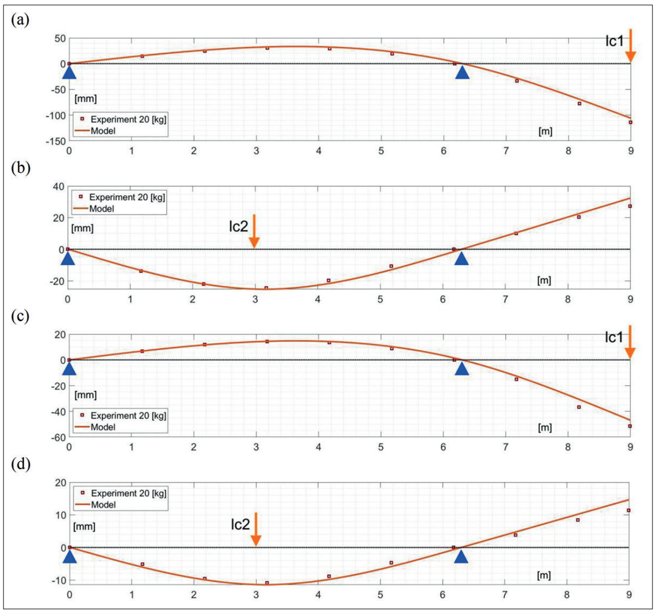

Fig. 13. Comparison of displacements obtained in experiment and FEM model: (a, b) along S direction, (c, d) along F/A direction

The difference between the values of the displacement at the measurement points and in the model does not exceed 29%. Analysing the top of the mast (point *u*8 or *v*8), it can be observed that for both orientations of the cross-section, the absolute values of displacement obtained for load case *lc*1 are greater for the real mast than for the mast model. However,

Tab. 5. Comparison of values at points v1–v8 under load schemes lc1 and lc2 for cross-section along the S direction

	p	*v*1	*v*2	***v*3**	*v*4	*v*5	*p*	*v*6	*v*7	***v*8**
	-	[mm]	[mm]	**[mm]**	[mm]	[mm]	-	[mm]	[mm]	**[mm]**
*lc*1										
Experiment [mm]	-	14.78	24.75	**30.12**	28.90	19.36	-	-33.42	-77.82	**-114.13**
Model [mm]	-	15.45	26.21	**32.46**	32.12	23.10	-	-28.57	-69.32	**-106.17**
Relative error [%]	-	4.53	5.90	**7.77**	11.14	19.33	-	-14.51	-10.92	**-6.97**
*lc*2										
Experiment [mm]	-	-13.83	-21.92	**-24.39**	-19.69	-10.69	-	10.08	20.29	**27.21**
Model [mm]	-	-13.39	-21.96	**-25.34**	-21.69	-12.96	-	10.49	22.49	**32.38**
Relative error [%]	-	-3.18	0.18	**3.90**	10.16	21.23	-	4.07	10.84	**19.00**

Tab. 6. Comparison of values at points u1–u8 under load schemes lc1 and lc2 for the cross-section along the F/A direction

	p	*u*1	*u*2	***u*3**	*u*4	*u*5	*p*	*u*6	*u*7	***u*8**
	-	[mm]	[mm]	**[mm]**	[mm]	[mm]	-	[mm]	[mm]	**[mm]**
*lc*1										
Experiment [mm]	-	6.77	11.82	**14.16**	13.54	8.89	-	-15.17	-36.71	**-51.38**
Model [mm]	-	6.86	11.64	**14.41**	14.26	10.25	-	-12.64	-30.65	**-46.89**
Relative error [%]	-	1.33	-1.52	**1.77**	5.32	15.30	-	-16.68	-16.51	**-8.74**
*lc*2										
Experiment [mm]	-	-5.11	-9.56	**-10.88**	-8.85	-4.70	-	3.84	8.46	**11.38**
Model [mm]	-	-6.04	-9.91	**-11.43**	-9.79	-5.85	-	4.75	10.17	**14.65**
Relative error [%]	-	18.20	3.66	**5.06**	10.62	21.47	-	23.70	20.21	**28.73**

for load case *lc*2, the deflection is higher for the model than for the real structure.

Moreover, regarding the stress level, for *lc*1, an extreme stress level was obtained in the vicinity of the mid-support. The values exceeded 22.6 MPa and 37.9 MPa for cross-section orientation along the F/A and S directions, respectively. However, for *lc*2, extreme stresses occurred in the area where the force was applied, which is between supports; these stresses were equal to 13.01 MPa and 24.49 MPa for cross-section orientation along the F/A and S directions, respectively. The extreme values of stress obtained in the model were about 3.8% and about 5.2% for the strength of the material given in Table 2, considering the F/A and S directions, respectively. Thus, this fulfils the assumption mentioned earlier that the stresses are well below FI < 0.2 (i.e. according to Tsai-Wu), and the suitability of the mast for sailing is determined by its stiffness, not its load-bearing capacity.

SENSITIVITY ANALYSIS

INTRODUCTION

A numerical model created to describe the behaviour of a real structure can be expressed by parameters divided into three groups: design variables b_i, which are given by the designer and can vary (i.e. dimensions of cross-section or material parameters); model parameters p_j, which are fixed and cannot be changed by the designer (i.e. span length of the bridge defined by the obstacle it crosses); and state variables S_k, which are structural responses (i.e. internal forces, stresses, strains, or dynamic parameters). Structural analysis aims to determine state variables S_k when design variables b_i and model parameters p_j are given. However, in practice, the task is often inverse – the designer expects a certain range of values of state variables S_k (i.e. the level of stresses or displacement), while design variables b_i are selected to ensure this; the model parameters p_j are imposed. In order to fulfil these requirements, the designer can use sensitivity analysis, which is one of the branches of the inverse problem. Thus, the purpose of sensitivity analysis is to determine the impact of the variation of design variables δb_i on the variation of state variables δS_k, assuming fixed model parameters p_j. This relationship can be described by the following equation:

$$\delta S = \mathbf{w}_S\, \delta \mathbf{b}\ , \tag{1}$$

where $\mathbf{w}_S = \{w_1, w_2, \dots , w_n\}$is a sensitivity vector containing sensitivity coefficients w_i, and $\delta\mathbf{b} = \{\delta b_1, \delta b_2, \dots , \delta b_n\}^T$ is a vector of variations of design variables δb_i. When solving sophisticated problems using commercial software, without access to the internal source and, e.g. the implicit character of the stiffness or mass matrix of the structure, the sensitivity coefficients may be determined with the use of the central difference equation:

$$w_i = \frac{\frac{S(b_{0,i} + \Delta b_i)}{S_0} - \frac{S(b_{0,i} - \Delta b_i)}{S_0}}{\frac{2\Delta b_i}{b_{0,i}}}\ , \tag{2}$$

where $S_0 = S_0(b_{0,i})$ is a state variable value obtained for the initial value of a design variable $b_{0,i}$, Δb_i is the variation of a chosen design variable, and $S = S(b_{0,i} + \Delta b_i)$ is a state variable value received with the updated value of the design variable $b_{0,i} + \Delta b_i$.

DESCRIPTION OF NUMERICAL EXAMPLE

The paper consists of an example of sensitivity analysis conducted on the validated model of the mast. The aim is to determine how to modify the mast to obtain the expected global stiffness of the structure, i.e. to obtain the expected displacement of the mast along its length. For this purpose, the displacement of chosen points along the structure was assumed as state variables, while the thickness of the cross-section walls was assumed as design variables. Sensitivity analysis is used to determine the impact of the variation of the thickness of cross-section walls on the variation of the displacement of the mast.

Due to the cross-section shape, the stiffness differs significantly along different directions – along the F/A direction, the stiffness is relatively high, while along the S direction, it is relatively low. This is why the cross-section walls are strengthened with additional laminate layers in the S direction (see Fig. 2a), and hence the cross-section has two values of wall thickness – $t1$ (not strengthened) and $t2$ (with additional layers). For this reason, sensitivity analysis was conducted only along the S direction, where displacement along the y-axis (v-axis) and a thickness $t2$ are assumed as a state variable and a design variable, respectively.

In order to perform more precise multiparameter sensitivity analysis, the structure was additionally divided into 20 segments with equal lengths of 45 cm. In each segment, the thicknesses of the cross-section wall $t1$ and $t2$ can be assumed separately, which leads to 40 independent areas (Fig. 14). However, only $t2$ thicknesses were considered as design variables, while $t1$ thicknesses were considered as model parameters and were constant. Thus, the vector of design variables can be expressed as $\mathbf{b} = \{t2_1; t2_2; t2_3; \ldots ; t2_{20}\}$. As mentioned before, the SLS is a more significant requirement to analyse for the composite mast than the ULS; hence, displacements were assumed as a state variable. Moreover, to obtain more precise results, eight points were considered that were located in the same places as the measurement points $v1-v8$ along the S direction – at a distance of about 1 m from each other.

RESULTS

In order to compute sensitivity vector coefficients, the assumption was made that the elements of a design variable vector could independently vary from -50% to +50% with respect to their initial values. Thus, the thickness $t2$ of cross-section walls ranges from 1.75 mm to 5.25 mm. Only one state variable and one load case can be assumed in one sensitivity analysis computation; hence, 16 calculation rounds were conducted. Thus, 16 sensitivity coefficient vectors were computed according to Eq. (2), for different state variables $\mathbf{S} = \{v1; v2; v3; \ldots ; v8\}$ and load schemes ($lc1$ and $lc2$). As a result, two matrices of sensitivity coefficients were obtained:

$$w_{k,i}^{lc1} = \begin{bmatrix} w_{1,1}^{lc1} & w_{1,2}^{lc1} & \ldots & w_{1,20}^{lc1} \\ w_{2,1}^{lc1} & w_{2,2}^{lc1} & \ldots & w_{2,20}^{lc1} \\ \ldots & \ldots & \ldots & \ldots \\ w_{8,1}^{lc1} & w_{8,2}^{lc1} & \ldots & w_{8,20}^{lc1} \end{bmatrix} \text{and} \quad w_{k,i}^{lc2} = \begin{bmatrix} w_{1,1}^{lc2} & w_{1,2}^{lc2} & \ldots & w_{1,20}^{lc2} \\ w_{2,1}^{lc2} & w_{2,2}^{lc2} & \ldots & w_{2,20}^{lc2} \\ \ldots & \ldots & \ldots & \ldots \\ w_{8,1}^{lc2} & w_{8,2}^{lc2} & \ldots & w_{8,20}^{lc2} \end{bmatrix}, \tag{3}$$

which can be expressed graphically as sensitivity lines that describe the impact of the variation of design variables (variation of the thicknesses $\delta t2_1-\delta t2_{20}$) on the variation of state variables (variation of the displacements $\delta v1-\delta v8$).

As an example, Fig. 15a shows a graphical representation of the sensitivity coefficient vector $w_{3,i}^{lc1}$ in two ways. The bars present the values of sensitivity coefficients, whereas the line (so-called sensitivity line) was obtained by connecting adjacent values. Both graphs present the impact of the variation of 20 design variables (the thickness $t2$ in each segment) on the variation of the state variable – displacement $v3$ in the middle, between supports, for load scheme $lc1$. The highest value of the sensitivity coefficient was obtained for the eighth segment and was equal to -4.2%, which means that an increase in the thickness $t2$ by 50% in the eighth segment results in a decrease in displacement $v3$ by 4.2%. It can be observed that the graph is not symmetric – the higher values of sensitivity coefficients were obtained closer to the mid-support in the ninth to the twelfth segments. On the other hand, at the mast top, the sensitivity coefficients are equal to zero, which means that the variation of thickness $t2$ in those areas does not result from a change in displacement $v3$.

In the same way, the sensitivity coefficient vector $w_{8,i}^{lc1}$ for design variable $v8$ (the displacement at the mast top) is presented in Fig. 15b. The highest value of the sensitivity coefficient was obtained in the fourteenth segment, which is near the mid-support, and was equal to -4.1%. An increase in the thickness $t2$ by 50% in this area results in a decrease in the displacement of the mast top by 4.1%.

In order to obtain a graphical representation of the whole sensitivity coefficient matrix $w_{k,i}^{lc1}$ for load scheme $lc1$, the results for all eight design variables (displacement of points $v1-v8$) were plotted on a single graph in Fig. 15c by means of sensitivity lines. The graph gives an overall view of where sensitivity coefficients are higher and where they are lower compared to each other. Thus, it can be used to determine which areas need to be strengthened, i.e. by adding an extra layer of laminate, and which may be made thinner by omitting one layer of laminate, to minimise or maximise the chosen displacement along the mast.

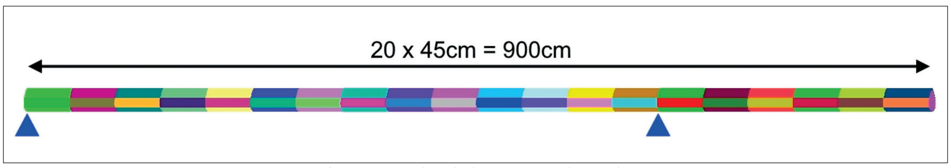

Fig. 14. The mast is divided into 40 independent areas

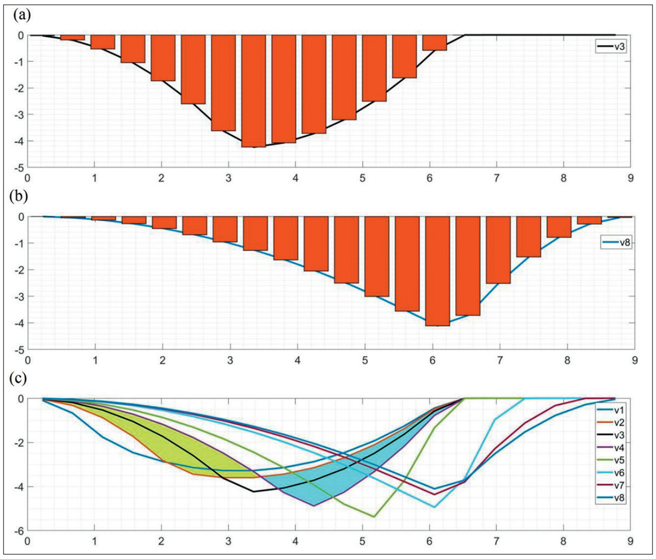

Fig. 15. Sensitivity lines for lc1, for the following state variables: (a) only v4, (b) only v8, (c) v1–v8

Moreover, based on the graph (Fig. 15c), the shape of the deformed mast may be designed as well. The basic deformation of the mast caused by load scheme *lc*1 is presented in Fig. 13a. For example, to obtain a quasi-symmetric deformation of the mast between both supports, the values of chosen displacements *v*2 and *v*4 have to be similar, which means that displacement *v*2 has to be increased while displacement *v*4 decreases. To fulfil this assumption, the sensitivity lines for state variables *v*2 and *v*4 have to be taken into account and compared. In the area coloured yellow, the sensitivity coefficients for state variable *v*2 are higher than those for state variable *v*4. Thus, reducing the thickness *t*2 of the segments located here would cause the value of displacement *v*2 to increase compared to *v*4. On the other hand, in the area coloured light blue, the sensitivity coefficients are higher for state variable *v*4 than for *v*2. This means that strengthening segments located here would cause displacement *v*4 to decrease compared to *v*2. Both actions would cause the deformation of the mast to be more symmetric.

The graphical representation of the whole sensitivity coefficient matrix $w_{k,i}^{lc2}$ for load scheme *lc*2, which consists of sensitivity coefficients computed for all eight design variables (*v*1–*v*8), was plotted in Fig. 16. The highest value of the sensitivity coefficient was obtained for state variable *v*3 and exceeded about -5.8% in the middle between two supports. On the other hand, at the mast top, the value of the sensitivity coefficients is equal to 0, which means that the variation of the thickness *t*2 along the mast does not impact the variation of any state variable.

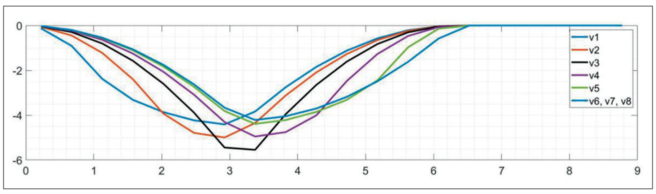

Fig. 16. Sensitivity lines for lc2, for all state variables v1–v8

CONCLUSIONS

This article focuses on the experimental and numerical study of the stiffness of an A-class catamaran (A-Cat) mast. The work includes the determination of the material parameters of the mast and experimental studies of the entire mast. The behaviour of the mast under two static loads was investigated. The tests indicate the bending of the mast, which is a commonly used test performed by mast manufacturers and professional users. The studies allow us to determine the bending stiffness of the mast, a key parameter in the design process of a boat or yacht's mast and sail. The paper also utilised numerical modelling, specifically finite element modelling (FEM), to simulate the behaviour of the mast under two loading conditions as it was examined during experiments. This allowed the validation of the computational model.

The main element of the paper was the use of a sensitivity analysis apparatus to determine the influence of changes in the stiffness of individual mast areas on their global response, i.e. the displacement of selected points along the length of the structure. The thickness of mast segments was systematically varied, leaving the mast geometry (e.g. cross-sectional shape, support location) unchanged. The study revealed which areas of the mast have the greatest and least impact on the selected lateral displacement of the mast, and therefore its stiffness. The paper also presents an example of where the mast cross-section should be strengthened and where it should be weakened to achieve the desired bending deflection line, for example, in the form of a symmetrical curve.

The example presented in the article demonstrates the importance of correct mast design through the precise selection of appropriate parameters affecting the mast's flexural stiffness. The example provides practical recommendations for designers, indicating the need for a sensitivity analysis, which makes it possible to improve the mast design process, taking into account the stiffness parameters expected by high-performance sailors. The results obtained in the presented bending tests might be a starting point for further analysis of the behaviour of the mast, where the stiffness of the mast and its interaction with the sail directly influence the sporting performance. Further analysis can be conducted, e.g. by means of fluid–structure interaction (FSI) analyses. The presented method can support designers in developing more efficient and competitive masts for sailing yachts.

CRediT author statement

Tomasz Ferenc: *Conceptualization, Methodology, Investigation, Software, Data Curation, Writing - Original Draft*

Tomasz Mikulski: *Conceptualization, Methodology, Investigation, Writing - Review & Editing, Supervision*

ACKNOWLEDGEMENT

The authors would like to thank Mr Jakub Kopyłowicz from the company Exploder (Rokitki, Poland) for his help in carrying out the experimental research.

REFERENCES

1. Larsson L, Eliasson R, Orych M. Principles of yacht design. International Marine/Ragged Mountain Press; 2014.

2. Killing S, Hunter D. Yacht design explained: A boat owner's guide to the principles and practice of design. International Marine/Ragged Mountain Press; 2012.

3. Skene NL. Elements of yacht design. Dodd, Mead & Company; 1977.

4. Perry R. Yacht design according to Perry: My boats and what shaped them. Sheridan House; 2008.

5. Graf K, Freiheit O, Schlockermann P, Mense JC. VPP-driven sail and foil trim optimization for the Olympic NACRA 17 foiling catamaran. J Sail Technol 2020. https://doi.org/10.5957/jst/2020.5.1.61.

6. Knudsen SS, Marimon Giovannetti L, Legarth BN, Walther JH. Dynamic fluid structure interaction of NACRA 17 foil. J Mar Sci Eng 2024. https://doi.org/10.3390/jmse12020237.

7. Masuyama Y, Ogihara M. Science of the 470 sailing performance. J Sail Technol 2020. https://doi.org/10.5957/jst.2020.5.1.20.

8. Lin S, Ma Y, Zheng W, Pan Z. Numerical simulation of mutual influence in 470 sailing hull and rudder at different hull speeds. Proceedings of the 13th Conference of the International Sports Engineering Association, 2020. https://doi.org/10.3390/proceedings2020049134.

9. Cella U, Cucinotta F, Sfravara F. Sail plan parametric CAD model for an A-class catamaran numerical optimization procedure using open source tools. In: Eynard, B., Nigrelli, V., Oliveri, S., Peris-Fajarnes, G., Rizzuti, S. (eds) Advances on Mechanics, Design Engineering and Manufacturing . Lecture Notes in Mechanical Engineering. Springer, Cham 2017. https://doi.org/10.1007/978-3-319-45781-9_55.

10. Keller T, Henrichs J, Hochkirch K, Hochbaum AC. Numerical simulations of a surface piercing A-class catamaran hydrofoil and comparison against model tests. J Sail Technol 2017. https://doi.org/10.5957/jst.2017.04.

11. Samson L, Kahsin M. A method to determine the tightening sequence for standing rigging of a mast. Polish Marit Res 2019. https://doi.org/10.2478/pomr-2019-0065.

12. Gama Caetano D, Scandiuzzi Valença de Castro D, Giron Camerini C, Kotik H G, Alho A. Failure analysis of a CFRP mast of a racing sailboat. Eng Fail Anal 2023. https://doi.org/10.1016/j.engfailanal.2023.107263.

13. Ghelardi S, Conti C, Gaiotti M, Rizzo C M, Paci M. Scantling assessment of large yacht rigs using carbon-fiber and aluminum masts. Ocean Eng 2019. https://doi.org/10.1016/j.oceaneng.2019.106480.

14. Mechin P-Y, Keryvin V. Analysis on the key parameters driving the mast stiffness accuracy to improve sail design using fluid/structure simulation with beam elements. J Sail Technol 2024. https://doi.org/10.5957/jst/2024.9.1.57.

15. Samson L, Kahsin M. A method to determine the tightening sequence for standing rigging of a mast. Polish Marit Res 2019. https://doi.org/10.2478/pomr-2019-0065.

16. Bak S, Yoo J. FSI analysis on the sail performance of a yacht with rig deformation. Int J Nav Archit Ocean Eng 2019. https://doi.org/10.1016/j.ijnaoe.2019.02.003.

17. Bak S, Yoo J, Song C Y. Fluid-structure interaction analysis of deformation of sail of 30-foot yacht. Int J Nav Archit Ocean Eng 2013. https://doi.org/10.2478/IJNAOE-2013-0131.

18. Sacher M, Leroux J-B, Nême A, Jochum C. A fast and robust approach to compute nonlinear fluid-structure interactions on yacht sails – Application to a semi-rigid composite mainsail. Ocean Eng 2020. https://doi.org/10.1016/j.oceaneng.2020.107139.

19. Augier B, Bot P, Hauville F, Durand M. Experimental validation of unsteady models for fluid structure interaction: Application to yacht sails and rigs. J Wind Eng Ind Aerodyn 2012. https://doi.org/10.1016/j.jweia.2011.11.006.

20. Lou B, Cui H. Fluid–structure interaction vibration experiments and numerical verification of a real marine propeller. Polish Marit Res 2021. https://doi.org/10.2478/pomr-2021-0034.

21. Kozak J, Tarełko W. Case study of masts damage of the sail training vessel POGORIA. Eng Fail Anal 2011. https://doi.org/10.1016/j.engfailanal.2010.11.016.

22. Song C-Y. Enhancement of shipboard radar mast vibration performance by adopting design sensitivity analysis and topology optimization. Ocean Eng 2025. https://doi.org/10.1016/j.oceaneng.2024.120253.

23. Ferenc T. Multiparameter sensitivity analysis of a GFRP composite footbridge of a sandwich structure and U-shaped cross-section. Compos Struct 2020. https://doi.org/10.1016/j.compstruct.2020.112793.

24. Ferenc T, Gierasimczyk R, Mikulski T. Stress assessment of a steel bullet LPG tank under differential settlement based on geodetic measurements and sensitivity analysis. Polish Marit Res 2024. https://doi.org/10.2478/pomr-2024-0056.

25. Harris B. Engineering composite materials. The Institute of Materials, London; 1999.

26. Lemaitre J. Handbook of materials behavior models. Academic Press; 2001.

27. Tsai SW, Wu EM. A general theory of strength for anisotropic materials. J Comp Mater 1971. https://doi.org/10.1177/002199837100500106.

28. Tsai SW, Hahn HT. Introduction to composite materials. Technomic Publishing Co.; 1980.